Available online at www.sciencedirect.com
ScienceDirect
Journal of Power Sources 161 (2006) 782–789
JOURNAL OF POWER SOURCES
www.elsevier.com/locate/jpowsour

Pt-, PtNi- and PtCo-supported catalysts for oxygen reduction in PEM fuel cells

N. Travitsky [a], T. Ripenbein [a], D. Golodnitsky [a], Y. Rosenberg [b], L. Burshtein [b], E. Peled [a,*]

[a] *School of Chemistry, Sackler Faculty of Exact Sciences, Tel Aviv University, Tel Aviv 69978, Israel*
[b] *Wolfson Applied Materials Research Center, Tel Aviv University, Tel Aviv 69978, Israel*

Received 16 March 2006; accepted 23 May 2006
Available online 27 June 2006

Abstract

The most widely used supporting material for ORR catalysts is high-surface-area carbon (such as Vulcan XC-72). However, at elevated temperatures, burning of the carbon-to-catalyst contact takes place and drying out of the cathode may destroy the three-phase zones. In order to avoid these problems, Pt catalysts supported on silica were synthesized and characterized parallel to those supported on carbon. In a search for more active and stable catalysts, in addition to supported Pt powders, we have synthesized and characterized carbon- and silica-supported PtNi and PtCo catalysts via the same electroless-deposition route. In order to avoid agglomeration of the platinum particles, a classic three-step electroless deposition (sensitization and activation, nucleation and growth) on silica and XC-72 was used for the first time. The PtNi- and the PtCo-supported catalysts have smaller crystal size (as low as 2.2 nm) and larger electrochemical surface area (up to 57 $m^2\ g^{-1}$) than do pure Pt-supported catalysts. The stability of the alloy catalysts in acidic medium was tested. Catalysts post-treated in acid were found to be stable and had a platinum-rich (or pure) "skin" structure. Some conclusions were drawn regarding catalyst structure and corrosion mechanism.

Keywords: Supported; Platinum; Cobalt; Nickel; Catalyst; Fuel cell

1. Introduction

Polymer-electrolyte fuel cells (PEFCs) have attracted great attention due to their high power density, low-temperature operation and environmentally friendly technology. Nano-sized platinum catalysts are used both in the cathode and in the anode of the PEFC. In order to reduce cathode-activation losses due to the comparably sluggish kinetics of the oxygen reduction reaction, more active catalysts should be used [1–3]. One way to improve cathode performance is to use supported Pt catalysts that have higher surface area and lower platinum loading [4–9]. Further improvement, related to the reduction of the activation potential of the cathode and at the same time to lowering its price, can be achieved by using Pt-based alloys with transition metals. It has been reported that Pt alloyed with Ni, Co, Cr, Fe and Mn enhances the electrocatalytic activity for the oxygen reduction reaction (ORR) by up to several orders of magnitude [10–16]. The most promising type of catalyst is a Pt "skin" alloy catalyst containing mainly platinum in the first few atomic layers [17]. The stability of alloy catalysts depends strongly on the harsh working conditions of the fuel cell. Transition metals dissolve from the platinum alloy both in the phosphoric acid fuel cell and in acidic membrane cells during operation, as shown by many research groups [1,18–20]. This is followed by a reduction in catalyst activity. In addition, the leached metal atoms can lower the conductivity of the proton-exchange membrane [1] and clog the GDL (gas diffusion layer) pores [21].

The most widely used catalyst-supporting material is high-surface-area carbon (Vulcan XC-72). However, at elevated temperatures, burning of the carbon-to-catalyst contact takes place. It has been found that the platinum particles are able to catalyze the combustion of the carbon support even at moderate temperatures (125–195 °C) [22]. Moreover, drying out of the cell at high temperatures may destroy the three-phase zones in the electrode and thus adversely affect cell performance. In order to avoid these problems, we suggest binding the Pt catalyst to a hydrophilic nano-sized ceramic powder such as silica. The platinum–silica bond is expected to be more stable than

* Corresponding author. Tel.: +972 3 6408438; fax: +972 3 6414126/6409293.
E-mail address: peled@post.tau.ac.il (E. Peled).

0378-7753/$ – see front matter © 2006 Elsevier B.V. All rights reserved.
doi:10.1016/j.jpowsour.2006.05.035

Pt–carbon at high temperatures, since Pt/SiO_2 catalysts are used effectively in exhaust gas after-treatment techniques at temperatures higher than 150 °C [23–26]. Furthermore, silica, with its hydrophilic properties, should improve catalyst-layer wetting and reduce the activation overpotential caused by proton deficiency in the three-phase zone. Electron conductivity could be provided by adding carbon to the catalyst ink of the cathode. With the aim to avoid agglomeration of the platinum particles, a classic three-step electroless deposition (sensitization and activation, nucleation and growth) on silica and XC-72 was used for the first time. It was found to be successful for carbon-supported catalysts while for silica-supported catalysts more work is needed. We report in this work synthesis and characterization of Pt-, PtNi- and PtCo-supported on silica and Vulcan XC-72. Corrosion of the alloy catalysts was studied and stable catalysts with high electrochemical surface area (ECSA) were obtained.

2. Experimental

2.1. Catalyst synthesis and characterization

The preparation of the supported catalysts was carried out by a classic electroless deposition process that included the following steps:

2.1.1. Activation–preparation of a submonolayer of Pt bonded to the carbon

Two grams of Vulcan XC-72 (Cabot) was added to 40 ml 0.4 M HCl and the slurry was sonicated for 30 min. Then, 0.64 g of $SnCl_2{\cdot}2H_2O$ and 3.2 g of KCl were added to the mixture which was then stirred for 10 min. After the XC-72 was washed thoroughly with HCl in a Buchner funnel to remove excess $SnCl_2$ (which did not adsorb on the carbon), it was transferred to 40 ml 0.4 M HCl. Then, 0.956 g of $PtCl_4$ was added to the solution and the mixture was stirred for 15 min. The carbon powder obtained was washed, centrifuged and dried by evaporation.

2.1.2. Synthesis

The carbon, covered by a submonolayer of Pt, was sonicated in 100 ml of distilled water for 30 min. $PtCl_4$ (and $NiCl_2{\cdot}6H_2O$ or $CoCl_2{\cdot}6H_2O$ in the case of alloy catalysts) was added and the mixture was stirred for 10 min. Then, 10 ml of ammonia was added in 2 ml portions with stirring to reach a final pH of 11. $NaBH_4$ was dissolved in 10 ml H_2O and rapidly added to the mixture. It was assumed that, at this point, all the metal ions dissolved in the solution have been reduced and deposited on the substrate. The catalytic powder obtained was recovered by centrifugation, treated in 1 M H_2SO_4 at 80 °C for 1 h (this last step was carried out only for Pt catalysts but not for Pt alloys), washed with distilled water until no chloride ions could be detected (in order to prevent reduction of the ORR activity [27]), and dried by evaporation. The same procedure was applied in the case of silica-supported catalyst powders, where SiO_2 (Aerosil 130, Degussa) was used instead of XC-72.

2.2. Catalyst characterization

X-ray diffraction (XRD) analysis was carried out with the use of a Theta–Theta Scintag powder diffractometer equipped with a Cu Kα source (λ = 1.5406 Å) and a liquid-nitrogen-cooled germanium solid-state detector. The mean size of coherent scattering domains ("grain" size) of the catalyst powders was estimated by the Scherrer equation [28] for the width of the (1 1 1) Bragg reflection, corrected for instrumental broadening.

Catalyst-particle size and distribution were also investigated by transmission electron microscopy (TEM) on a Tecnai F20 (FEI) with a 200 kV field-emission gun. The powder samples were sonicated in ethanol and put on a carbon grid (SPI). High-resolution scanning electron microscope (SEM) micrographs of the catalyst powders were recorded with a JEOL JSM 6700F. Alloy compositions were determined by energy dispersive X-ray spectroscopy (EDS) elemental analysis by means of an X-ray LINK detector with a Pentafet window coupled to a scanning electron microscope (JEOL JSM-6300). Unless otherwise specified, all catalyst compositions presented in the text are those resolved by EDS. XPS analysis was performed with a Philips UHV-5600 apparatus with an Al Kα emission source.

2.3. Electrode preparation and characterization

Cyclic-voltammetry tests were performed in a three-compartment glass cell. The working-electrode support was a 10 mm × 60 mm graph-foil (Hanita) with the edge surfaces coated by polyvinylidene fluoride (PVDF) except for a 65-mm^2 bare window. A measured amount of catalyst-powder suspension in deionized water was sonicated for an hour and immediately pipetted on the bare part of the foil. In the case of silica-supported catalysts, an amount of XC-72 equal to 10% (w/w) of the catalyst weight was added to the suspension. The catalyst area was about 50 mm^2. After drying the foil at 130 °C, about 20 mg of a Nafion solution diluted by ethylene glycol (EG) and isopropanol to concentrations ranging from 0.17 to 2.5% by weight was spread over the catalyst. Final drying and curing was performed at 130 °C for 30 min. The graphite foil electrode was held in a glass holder. Pd wire was used as a counter electrode and Ag/AgCl/3 M KCl (Metrohm) in a Luggin capillary compartment, as a reference electrode. All the potentials in this manuscript are relative to that of the Ag/AgCl reference electrode. All electrochemical experiments were carried out with the use of an Eco Chemie (Netherlands) AUTOLAB potentiostat at room temperature (24 ± 3 °C). Experimental data were collected by a computer using GPES manager software. Prior to cycling, the working electrode was held at 1 V for 10 s and then at 0.5 V for 10 s. Nitrogen was bubbled for 30 min before the measurements. The cell was cycled between −0.2 and 1.3 V at a 20 mV/s sweep rate. The voltammograms were reproducible from the third scan on. The electrochemical surface area of platinum was determined from the coulometric charge in the hydrogen-desorption region, under the assumption of 210 μC cm^{-2} of hydrogen adsorbed [29]. As the ECSA values were found to depend on the Nafion content, several tests with different amounts of Nafion were carried out until the opti-

mum value was found. This optimum value varied with the type of catalyst and the type of support and was in the range 10–30% Nafion. Excessively high Nafion loading may screen Pt particles and lower the measured ECSA. On the other hand, insufficient Nafion cannot properly bind catalyst to the electrode surface. The maximal values of ECSA are reported—they are an average of the two best results obtained with the optimal Nafion loading for each sample type. All values of ECSA are normalized to Pt loading: [$m^2\ g^{-1}$ (Pt)].

3. Results and discussion

3.1. Preparation procedure

The synthesis of carbon- and silica-supported catalysts is based on a well known electroless deposition method. While electrochemical reduction of the precursor platinum (and other metals) salts is widely used in the field of electrocatalyst preparation [30–34], we use a classic industrial process for producing metallic coatings on non-conducting surfaces. The purpose of using this multiple-stage process is to improve the distribution of platinum particles on the surface, to reduce agglomeration and to reduce catalyst grain size by creating separate catalytic islands.

The first step is surface sensitization with Sn:

$$\text{S–OH} + \text{Sn}^{2+} \rightarrow \text{S–OH} \cdot \text{Sn}_{\text{ads}}{}^{2+} \quad (1)$$

where S = C or Si.

It is followed by an activation step in which a Pt salt is added to the slurry, interchanged with Sn adsorbed on the support surface and chemically bonded to it:

$$2\text{S–OH} \cdot \text{Sn}_{\text{ads}}{}^{2+} + \text{Pt}_{\text{solution}}{}^{4+} \rightarrow (\text{S–OH})_2 \cdot \text{Pt}_{\text{ads}} + 2\text{Sn}_{\text{solution}}{}^{4+} \quad (2)$$

Eqs. (1) and (2) are schematic representations of the sensitization and nucleation steps.

The next step is the nucleation and growth of nano-platinum or platinum-alloy particles.

$$2\text{Pt}^{4+} + \text{BH}_4^- + 8\text{OH}^- \rightarrow \text{B(OH)}_4^- + 2\text{Pt} + 4\text{H}_2\text{O} \quad (3)$$

In 20% (w/w) platinum (or platinum alloy) catalysts supported on carbon, that are prepared by one-step electroless procedures, metal particles tend to agglomerate [30–32] and this leads to relatively small ECSAs determined by cyclic voltammetry (16–31 $m^2\ g^{-1}$ [30] and 16–51 $m^2\ g^{-1}$ [31]). Our homemade 60–65% (w/w) Pt and Pt alloy catalysts supported on Vulcan XC-72 had ECSAs of 18–57 $m^2\ g^{-1}$ (Table 1). In addition to those catalysts, 20% (w/w) PtCo/XC-72 was prepared and its ECSA was 68 $m^2\ g^{-1}$ (more details to be published). Salgado et al. [33,34], reported grain sizes of 3.8–7.9 nm (revealed by XRD) for 20% (w/w) Pt-Co catalysts produced by electroless deposition; our synthesized 65% (w/w) Pt-Co catalysts had grain sizes of 2.7–3.5 nm (Table 1).

The XPS spectrum (Fig. 1) of Pt 60% (w/w)/XC-72 indicates that no tin or boron is left on the catalyst surface after the preparation is complete, the latter contrary to the recent report which indicated boron deposition caused by the use of $NaBH_4$ during the electroless catalyst synthesis [32].

Table 1
Effect of alloying on Pt catalyst grain size and ECSA

Catalyst code	Catalyst composition by EDS[a]	Grain size	Maximal ECSA [$m^2\ g^{-1}$]	Lattice parameters[b] [Å]
BN5	Pt 65%/XC72	4.3	18	3.9151
BN13	$Pt_{51}Ni_{49}$ 65%/XC72	2.2	57	3.8486
BN15	$Pt_{48}Co_{52}$ 65%/XC72	2.7	32	3.8732
BT9	Pt 93%/SiO_2	5.8	3	3.9182
BT14	$Pt_{45}Ni_{55}$ 85%/SiO_2	3.2	6	3.8204
BT15	$Pt_{72}Co_{28}$ 85%/SiO_2	3.7	5	3.8767

[a] Weight percent of the metals is calculated from reagent concentrations.
[b] Pure metal lattice parameters: a_0(Pt) = 3.9231 Å; a_0(Ni) = 3.5238 Å; a_0(Co) = 3.5447 Å.

Despite relatively small grain size, the ECSA of silica-supported catalysts was found to be unexpectedly low. For example, the 93% (w/w) Pt/SiO_2 powder with 5.8 nm grain size has an ECSA of only 3 $m^2\ g^{-1}$. As visualized by TEM and HRSEM (Fig. 2), silica-supported Pt powder tends to agglomerate and this leads to the formation of large particles composed of small grains the sizes of which are determined by XRD. Thus, the total surface of the catalyst grains is not being utilized and there is no correlation between the electrochemical surface area measured by hydrogen desorption and the catalyst grain size. Another reason for the low values of ECSA could be the unoptimized electrode preparation and composition for the CV analysis. Although 10% XC-72 was added to the catalyst it may not be enough. This may lead to poor electrical contact between Pt particles and the electrode and underestimated catalyst surface. On the other hand, when a carbon support was used, lower grain size (4.6 nm) and higher ECSA (18 $m^2\ g^{-1}$) were obtained for a 60% Pt sample (Table 1).

3.2. Alloy catalysts

PtNi and PtCo (1:1) supported on silica and XC-72 powders with various metal loadings were synthesized by the same prepa-

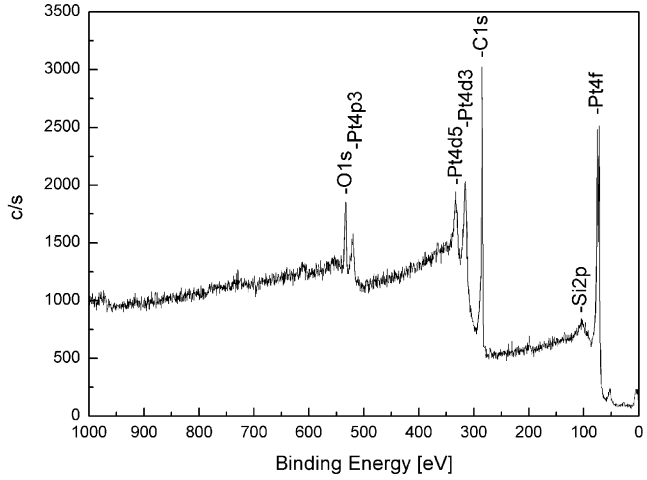

Fig. 1. XPS spectra of Pt 60% (w/w)/XC-72.

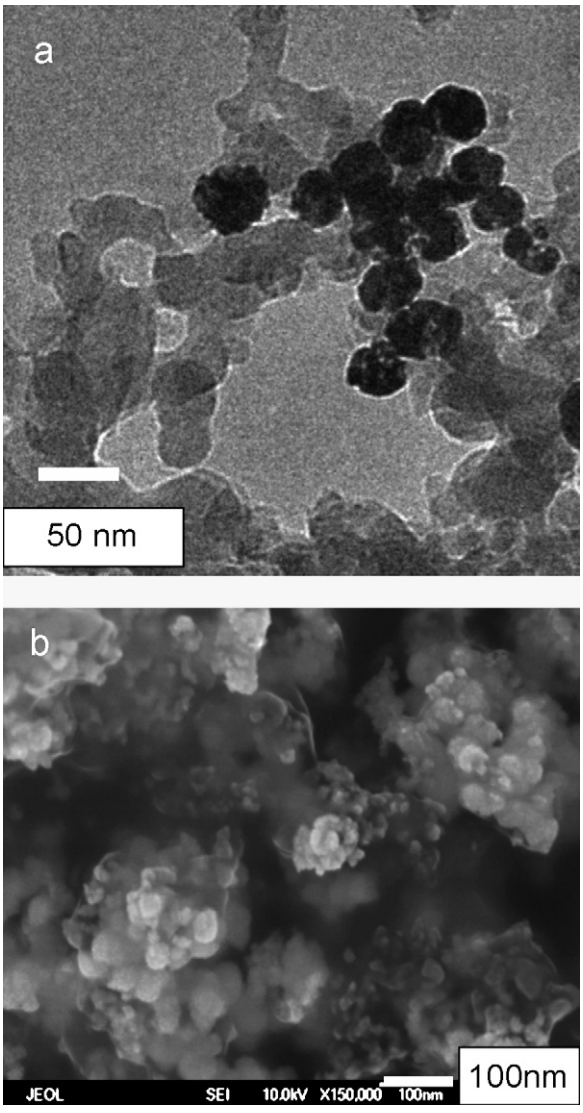

Fig. 2. (a) TEM micrographs of Pt 93% (w/w) /SiO_2 and (b) HRSEM micrograph $Pt_{45}Co_{55}/SiO_2$.

ration procedure. The effect of alloying on catalyst properties can be seen in Table 1. The grain size of silica-supported alloys is typically larger and ECSA is smaller than for XC-72-supported catalysts as in case of Pt catalysts. Alloying with nickel and cobalt led to reduction in grain size and higher ECSA. The equation for the relation between the catalyst spherical grain size and its surface area is [35]

$$S = \frac{6 \times 10^3}{\rho d} \tag{4}$$

where S is surface area ($m^2\,g^{-1}$), d the particle diameter and ρ is a metal lattice density. With this equation it is possible to estimate the effect of alloying on the degree of agglomeration. For carbon-supported catalysts the degree of reduction of the platinum-catalyst grain size that is caused by alloying with nickel and with cobalt is 4.3/2.2 and 4.3/2.7, respectively (Table 1). However, ECSA enhancement is more pronounced (57/18 for PtNi/XC-72 and 32/18 for PtCo/XC-72). It can be concluded

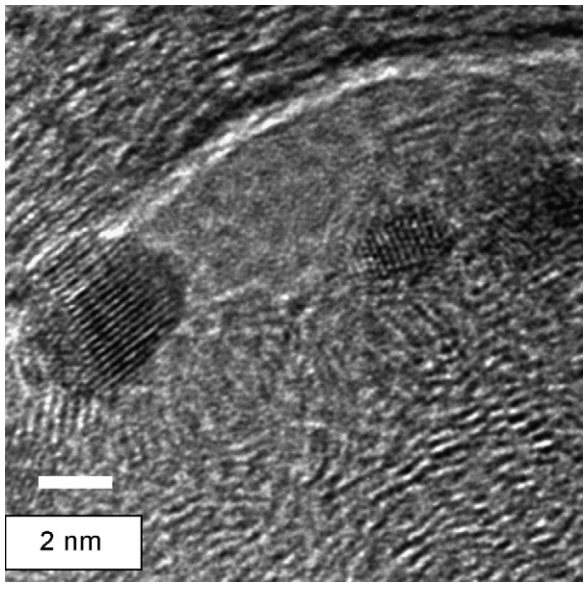

Fig. 3. TEM micrograph of $Pt_{69}Ni_{31}$ 65% (w/w)/XC72 magnified by 1,050,000.

that alloying platinum with nickel and cobalt not only lowers the grain size but also reduces the degree of agglomeration of the catalyst grains. This indicates that nickel eliminates agglomeration of nano-particles more effectively. This conclusion is supported by a TEM micrograph (Fig. 3) which shows discrete PtNi particles on carbon support. The decrease in agglomeration is attributed to the "anchoring effect" of nickel and cobalt on platinum. Platinum mobility on the supporting material is lowered as a result of the stronger bonding of the non-noble alloying metal atoms to the carbon powder, which in turn prevents sintering [1,19,36,37].

In SiO_2-supported catalysts, however, there is a correlation (according to Eq. (4)) between grain-size reduction and ECSA growth that results from alloying with nickel and cobalt. Thus, it can be deduced that the increase in ECSA is due only to particle-size reduction and that the degree of agglomeration does not change upon alloying. The effect of alloying on catalyst structure revealed by XRD can be seen in Fig. 4. The diffraction patterns indicate that all the alloys must be FCC binary solid solutions. No evidence was found of pure platinum, cobalt, nickel or any oxide

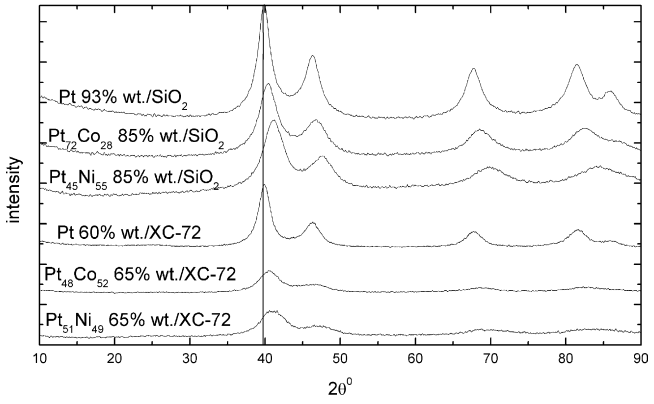

Fig. 4. XRD patterns of Pt- and Pt alloy-supported catalysts. Vertical line indicates 2θ diffraction angle of pure Pt.

Table 2
Effect of acid treatment on alloy-catalyst properties

Batch series	Catalyst treatment [nm]	Grain size	Maximal ECSA [$m^2\ g^{-1}$]	Composition		
				EDS	XRD	XPS
BN13	As-prepared	2.2	57	$Pt_{51}Ni_{49}$	$Pt_{87}Ni_{13}$	$Pt_{53}Ni_{47}$
	Treated	2.8	28	$Pt_{69}Ni_{31}$	$Pt_{87}Ni_{13}$	$Pt_{86}Ni_{14}$
BN15	As-prepared	2.7	32	$Pt_{48}Co_{52}$	$Pt_{87}Co_{13}$	$Pt_{37}Co_{63}$
	Treated	3.5	21	$Pt_{79}Co_{21}$	$Pt_{86}Co_{14}$	$Pt_{96}Co_4$
BT17	As-prepared	2.8		$Pt_{37}Co_{63}$	$Pt_{77}Co_{23}$	Pt_3Co_{97}
	Treated	4.0		$Pt_{61}Co_{39}$	$Pt_{82}Co_{18}$	$Pt_{80}Co_{20}$
E-TEK catalyst	As-prepared	3.4	69	$Pt_{48}Co_{52}$	$Pt_{68}Co_{32}$	$Pt_{45}Co_{55}$
	Treated	3.1	48	$Pt_{80}Co_{20}$	$Pt_{70}Co_{30}$	No Co was found

BN series catalysts (PtM 65% (w/w)/XC-72) and E-TEK catalyst (PtM 20% (w/w)/XC-72) were treated in 1 M H_2SO_4 80 °C, 15 h. While BT series catalyst (PtM 85% (w/w)/SiO_2) was treated in 1 M H_2SO_4, room temperature (RT), 24 h.

phases. The Bragg reflections shift slightly to higher diffraction angles indicating a decrease in the alloy lattice parameter during solid-solution formation. Substantial peak broadening is caused by reduction in the size of the crystal grains of the alloy catalysts.

Assuming the validity of Vegard's Law (the linear lattice constant–concentration relation) [38], one can estimate the compositions of the alloy catalysts under investigation. These results are shown in the sixth column of Table 2. As can be seen, there are systematic discrepancies between the alloy compositions estimated according to Vegard's Law and those found by EDS and XPS. This inconsistency might be caused, on the one hand, by deviations from linearity of the lattice constant–composition relation [39], in particular in the middle of the concentration range. On the other hand, XRD compositional analysis refers only to the crystalline part of the sample while EDS characterizes the entire sample volume and XPS probes thin surface layers. With this in mind, the XRD, EDS and XPS data can be reconciled provided that our as-prepared alloy catalysts comprise both ordered crystalline and disordered (amorphous) regions enriched with transition metals. It will be shown below that a corrosion study confirms this conclusion.

3.3. Investigation of alloy-catalyst corrosion

Since the cathode in a fuel cell is exposed to the corrosive environment of the acidic electrolyte and oxygen, the stability of the alloy catalysts must be studied. For this purpose, alloy catalysts supported on carbon and on silica were treated in 1–3 M H_2SO_4 at different temperatures and for various periods of time. It will be noted that in 0.5 M H_2SO_4 at room temperature, alloy catalysts are stable for at least a short period of time (about 1 h) at operating voltages of up to 1.5 V versus SHE as their cyclic voltammograms are similar to those of the platinum electrode. Furthermore, during five voltammetric scans of all the samples, no additional current peaks which could be attributed to alloying-metal corrosion were observed. The effect of corrosion on catalyst grain size and surface area can be seen in Table 2.

Typical XRD patterns of the as-prepared and treated PtNi catalysts are presented in Fig. 5(a). The narrowing of the (1 1 1) peak is caused by grain-size enlargement. In parallel, the ECSA of the treated catalyst is reduced, as seen in the cyclic voltammograms in Fig. 5(b). Acidic treatment (15 h 80 °C, Table 2) of the homemade platinum alloys led to a reduction of ECSA of about 42% and average grain-size enlargement of 30%, except for the

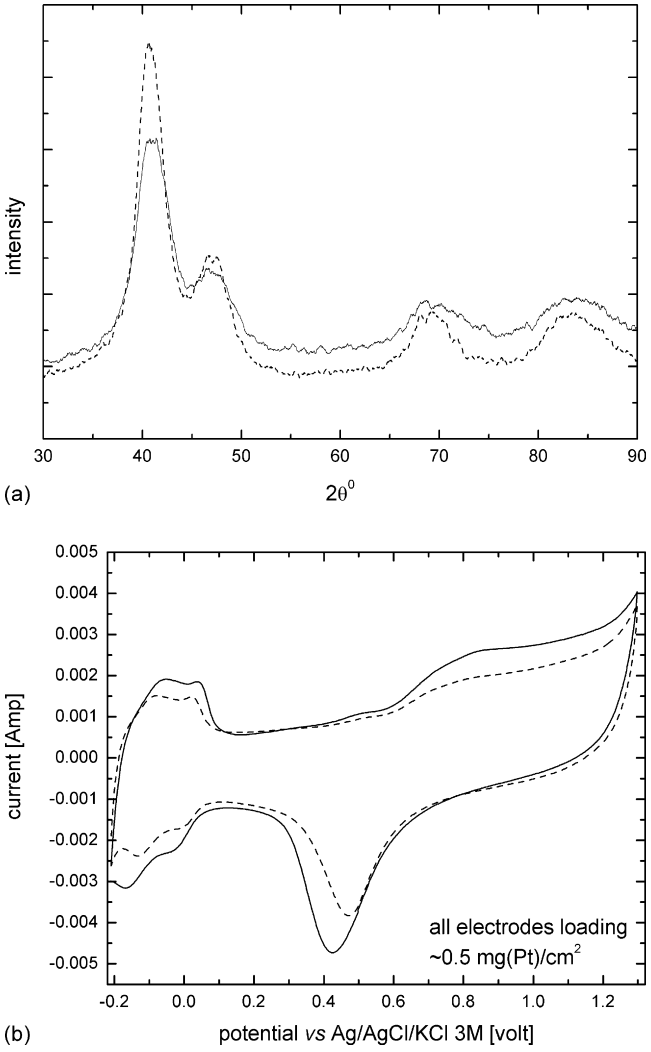

Fig. 5. (a) XRD pattern and (b) cyclic voltammogram of the as-prepared PtNi/XC-72 (solid line) and of the treated PtNi/XC-72 catalyst in 1 M H_2SO_4, 80 °C, 15 h (dotted line).

Table 3
Corrosion behavior of synthesized PtM/XC-72 catalysts

Catalyst code	Expected composition of as-prepared catalyst	Additional treatment[a]	Composition		Grain size [nm]
			EDS	XRD	
BN2	$Pt_{50}Ni_{50}$	–	$Pt_{69}Ni_{31}$	$Pt_{84}Ni_{16}$	3.3
		3 M, H_2SO_4, 80 °C, 3 h.	$Pt_{73}Ni_{27}$	$Pt_{84}Ni_{16}$	3.3
		3M, H_2SO_4, RT 24 h.	$Pt_{74}Ni_{26}$	$Pt_{84}Ni_{16}$	3.3
BN3	$Pt_{50}Co_{50}$	–	$Pt_{83}Co_{17}$	$Pt_{87}Co_{13}$	4.1
		3 M, H_2SO_4, 80 °C, 3 h.	$Pt_{88}Co_{12}$	$Pt_{87}Co_{13}$	4.2
		3M, H_2SO_4, RT 24 h.	$Pt_{85}Co_{15}$	$Pt_{87}Co_{13}$	4.2

[a] Both catalysts were preliminary treated in 3 M H_2SO_4, 80 °C for 1 h.

commercial catalyst, the grain size of which was reduced. Theoretically, one would expect that leaching of the alloying metal would leave a rougher surface, thus increasing the ECSA. However, the ECSA was reduced as a result of grain-size enlargement and probably the increase in the degree of agglomeration as well. In order to understand the reason for particle growth and sintering, the change of the catalyst composition during the corrosion test must be considered. The effect of acid treatment on the catalyst composition as found by various techniques is summarized in Table 2. Acid treatment leads to 40 and 40–60% reduction in the total concentrations of nickel and cobalt, respectively, both in the experimental and commercial catalysts. However, the lattice composition obtained from the XRD measurements does not change; the diffraction angles of the treated sample are similar to those of the as-prepared catalyst (Fig. 5(a)). The same is true for the PtCo catalyst. Consequently, it may be said that the catalyst crystal lattice is stable and that metal corrosion takes place outside the crystal lattice, in the amorphous regions of the catalyst particles. Thus, in order to prevent leaching of metal atoms, the number of amorphous regions must be reduced. This was done by acid treatment of the alloy catalysts for various periods of time (Table 3). It was found that after only 1 h in hot sulfuric acid, during which a significant amount of the alloying metal dissolves, corrosion is slowed and further acid treatments have little effect on catalyst composition. Similar results were presented in [19] during the accelerated durability test (ADT) of Pt_3Ni catalyst. Nickel dissolution stops at a composition of $Pt_{78}Ni_{22}$ and the catalyst diffraction pattern is not influenced by the ADT test.

Corrosion of the PtNi and PtCo carbon-supported alloys synthesized in this work as well as that of the commercial alloy, levels off at compositions of about Pt_2Ni and Pt_5Co. The crystal size becomes stable also after the 1 h treatment (Table 3). Thus, synthesized and treated alloy catalysts are stable in acidic environments. This is of great importance for fuel-cell applications as the leaching problem is resolved.

The proposed corrosion mechanism can also explain the crystal-size growth resulting from acid treatment. During the first 3 h, the dissolution of the amorphous regions lying between crystal lattices of PtNi or PtCo enables their recombination and recrystallization. Thus, when corrosion levels off, the grain size becomes stable. Since the decrease in ECSA as a result of acid treatment is greater than the grain-size enhancement, we may conclude that leaching of the amorphous regions leads to the increase in particle aggregation. However, the rise in the degree of agglomeration is relatively small and it lowers the ECSA by only 10% (Table 2), apparently as a result of the anchoring effect of nickel and cobalt. The corrosion mechanism in commercial catalysts seems to be different, as the crystal size decreases. The major difference between the synthesized and the E-TEK catalysts is a higher concentration of cobalt in the crystal lattice of the commercial powder. This could be due to the thermal treatment and would also explain the catalyst stability in 3 M H_2SO_4 at room temperature. However, the final composition (after 15-h corrosion tests) is similar to that of the synthesized PtCo powder.

SiO_2-supported catalysts responded in a similar manner to the sequence of acid treatments. After the first period, most of the amorphous phase was leached and further treatments resulted in no significant changes in either the total composition or the grain size (Table 4). There are two slight differences, however, between silica- and carbon-supported catalysts. A 24-h treatment at room temperature led to an unexpected decrease in the grain size of the PtNi silica-supported catalyst—a phenomenon that is hard to explain, since it differs from the behavior of other silica- and carbon-supported catalysts. In addition, the final average composition of the leached catalyst powders (only some of them are presented in Table 4) is similar for both alloying metals—Pt_2M. The slower corrosion of PtCo/SiO_2 powder as compared to the XC-72-supported catalyst can be explained in terms of stronger bonding between the cobalt atoms and the supporting material. In general, treated carbon-supported alloy catalysts are more stable in acidic environment than are silica-supported powders but the leaching of SiO_2-supported alloy

Table 4
Corrosion behavior of synthesized PtM/SiO_2 catalysts

Catalyst code	Treatment	Composition		Grain size [nm]
		EDS	XRD	
BT16	–	$Pt_{59}Ni_{41}$	$Pt_{82}Ni_{18}$	3.4
	1 M, H_2SO_4, 80 °C, 3 h	$Pt_{65}Ni_{35}$	$Pt_{87}Ni_{13}$	3.5
	1 M, H_2SO_4, 80 °C, 20 h	$Pt_{66}Ni_{34}$	$Pt_{84}Ni_{16}$	3.7
	1 M, H_2SO_4, RT, 24 h	$Pt_{69}Ni_{31}$	$Pt_{82}Ni_{18}$	2.2
BT17	–	$Pt_{37}Co_{63}$	$Pt_{77}Co_{23}$	2.8
	1M, H_2SO_4, 80 °C, 3 h	$Pt_{68}Co_{32}$	$Pt_{82}Co_{18}$	3.8
	1M, H_2SO_4, 80 °C, 20 h	$Pt_{73}Co_{27}$	$Pt_{84}Co_{16}$	4.4
	1M, H_2SO_4, RT, 24 h	$Pt_{64}Co_{36}$	$Pt_{80}Co_{20}$	3.7
	1M, H_2SO_4, RT, 170 h	$Pt_{61}Co_{39}$	$Pt_{82}Co_{18}$	4.0

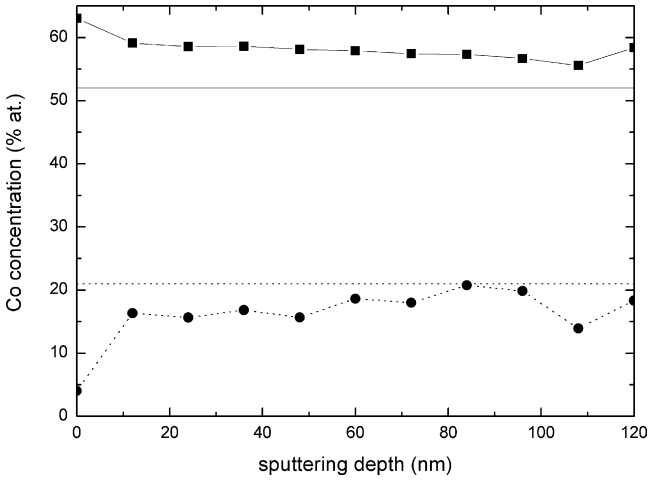

Fig. 6. Concentration profile of the PtCo/XC-72. Solid line—total concentration by EDS before treatment; squares—concentration by XPS before treatment; dotted line—total concentration by EDS after treatment and circles—concentration by XPS after treatment. Sputtering depth estimated by sputtering rate ∼6 nm/min.

catalysts takes a longer time, probably as a result of stronger bonding to the substrate.

The surface composition of the as-prepared alloy catalysts, shown by XPS analysis, is similar to that of the bulk (Fig. 6, Table 2). The treated sample surface is highly enriched in platinum. The cobalt concentration in the synthesized catalyst decreased by 95% (carbon-supported) and by 80% (silica-supported). In the E-TEK catalyst, no cobalt was found on the surface of the acid-treated catalyst. In the PtNi/XC-72 sample, the nickel concentration also decreased significantly (by 70%). Corrosion of nickel and cobalt took place on the surface of the catalyst particles, thus leaving a pure or almost pure platinum "skin". These "skin"-type catalysts are highly catalytic for the ORR reaction [13,17]. XPS analysis of the inner layers after sputtering of the samples showed that the concentration of the alloying metal increases sharply inside the sample and approaches the value given by EDS for the bulk concentration (Fig. 6).

This phenomenon can be explained in several ways. The explanation proposed by Watanabe [40], is that simultaneous dissolution of all the alloy components from the surface of small particles is followed by redeposition of platinum on the adjacent larger alloy particles. We propose another explanation. The catalyst surface consists mainly of a nickel-rich (or cobalt-rich) amorphous phase. Nickel (or cobalt) atoms dissolve from the surface of the particles, leaving platinum layers which stop further corrosion. Amorphous regions inside the particles cannot be leached when the platinum skin is formed. This explains the almost constant concentration of the alloy obtained after the first hot-acid treatment.

A few direct methanol fuel cells were assembled with the use of these platinum alloys as the cathode catalyst. They were fed by oxygen and operated at 130 °C. The maximal power density of these cells was 284 and 234 mW cm^{-2} for cells with 85% $Pt_{64}Co_{36}$ SiO_2 and 65% $Pt_{83}Co_{17}$ XC-72, respectively [41].

4. Conclusions

Silica- and carbon-supported platinum and platinum-alloy catalysts were synthesized by a classic three-step electroless deposition method. SiO_2-supported powders had larger grains and lower ECSAs than did the carbon-supported catalysts. This is due to the higher degree of agglomeration of their surface, which is attributed to the strong interaction of the metal particles with the silica support.

Alloying the platinum with cobalt and with nickel led to ∼40 and 50% reduction, respectively, in the grain size of both catalyst types. The ECSAs of carbon-supported catalysts increased by 100% when alloyed with cobalt and by more than 200% in the case of nickel. The enhancement of the ECSAs of the SiO_2-supported powders was comparable to the decrease in the grain size.

Corrosion of the transition metal led to increased grain size and lowered ECSA. Leaching of cobalt and nickel occurred on the surface of the catalyst particles to produce a platinum "skin"—a preferred structure for ORR. XRD and EDS analysis showed that only the cobalt and nickel atoms that are outside the crystal lattice dissolve, leaving stable catalysts.

References

[1] T.R. Ralph, M.P. Hogarth, Platinum Met. Rev. 46 (1) (2002) 3.
[2] J. Larminie, A. Dicks, Fuel Cell Systems Explained, John Wiley & Sons, Chichester, 2000.
[3] A. Freund, J. Lang, T. Lehmann, K.A. Starz, Catal. Today 27 (1996) 279.
[4] S. Lister, G. McLean, J. Power Sources 130 (2004) 61.
[5] D.A. Stevens, J.R. Dahn, J. Electrochem. Soc. 6 (2003) A770.
[6] A.S. Arico, S. Srinivasan, V. Antonucci, Fuel Cells 1 (2) (2001) 133.
[7] E.A. Ticianelli, E.R. Gonzalez, in: W. Vielstich, H.A. Gasteiger, A. Lamm (Eds.), Handbook of Fuel Cells—Fundamentals, Technology and Applications, vol. 2, John Wiley & Sons, Chichester, 2003, p. 490.
[8] H.G. Petrow, R.J. Allen, US Patent 4,044,193 (1977).
[9] L. Liu, C. Pu, R. Viswanathan, Q. Fan, R. Liu, E.S. Smotkin, Electrochim. Acta 43 (24) (1998) 3657.
[10] D.A. Landsman, US Patent 4,316,944 (1982).
[11] E. Antolini, Mater. Chem. Phys. 78 (2003) 563.
[12] S. Mukerjee, S. Srinivasan, M.P. Soriaga, J. McBreen, J. Electrochem. Soc. 142 (1995) 1409.
[13] V. Stamenković, T.J. Schmidt, P.N. Ross, N.M. Marković, J. Phys. Chem. B 106 (2002) 11970.
[14] T. Toda, H. Igrashi, H. Uchida, M. Watanabe, J. Electrochem. Soc. 146 (10) (1999) 3750.
[15] M. Min, J. Cho, K. Cho, H. Kim, Electrochim. Acta 45 (2000) 4211.
[16] E. Antolini, J.R.C. Salgado, E.R. Gonzales, J. Electroanal. Chem. 580 (2005) 145.
[17] V. Stamenković, T.J. Schmidt, P.N. Ross, N.M. Marković, J. Electroanal. Chem. 554–555 (2003) 191.
[18] B.C. Beard, P.N. Ross Jr., J. Electrochem. Soc. 137 (11) (1990) 3368.
[19] H.R. Colón-Mercado, H. Kim, B.N. Popov, Electrochem. Commun. 6 (2004) 795.
[20] T. Maoka, T. Kitai, N. Segawa, M. Ueno, J. Appl. Electrochem. 26 (1996) 1267.
[21] T. Itoh, US Patent 5,876,867 (1999).
[22] D.A. Stevens, J.R. Dahn, Carbon 43 (2005) 179.
[23] T.J. Schmidt, U.A. Paulus, H.A. Gasteiger, R.J. Behm, J. Electroanal. Chem. 508 (2001) 41.
[24] F. Jayat, C. Lembacher, U. Schubert, J.A. Martens, Appl. Catal. B 21 (1999) 221.
[25] R. Burch, D. Ottery, Appl. Catal. B 13 (1997) 105.

[26] J. Després, M. Elsener, M. Koebel, O. Kröcher, B. Schnyder, A. Wokaun, Appl. Catal. B 50 (2004) 73.
[27] J. Oi-Uchisawa, A. Obuchi, A. Ogata, R. Enomoto, S. Kushiyama, Appl. Catal. B 21 (1999) 9.
[28] B.E. Warren, X-Ray Diffraction, Addison-Wesley, Reading, MA, 1969.
[29] F.C. Nart, W. Vielstich, in: W. Vielstich, H.A. Gasteiger, A. Lamm (Eds.), Handbook of Fuel Cells—Fundamentals, Technology and Applications, vol. 2, John Wiley & Sons, Chichester, 2003, p. 302.
[30] J. Prabhuram, T.S. Zhao, C.W. Wong, J.W. Guo, J. Power Sources 134 (2004) 1.
[31] J.W. Guo, T.S. Zhao, J. Prabhuram, C.W. Wong, Electrochim. Acta 50 (2005) 1973.
[32] H.C. Ma, X.Z. Xue, J.H. Liao, C.P. Liu, W. Xing, Appl. Surf. Sci., in press.
[33] J.R.C. Salgado, E. Antolini, E.R. Gonzalez, J. Power Sources 138 (2004) 56.
[34] J.R.C. Salgado, E. Antolini, E.R. Gonzalez, J. Power Sources 141 (2005) 13.
[35] P. Stonehart, J. Appl. Electrochem. 22 (1992) 995.
[36] F.J. Luczak, US Patent 4,806,515 (1989).
[37] Z. Wei, H. Guo, Z. Tang, J. Power Sources 62 (1996) 233.
[38] R. Jenkins, R.L. Snyder, Introduction to X-Ray Powder Diffractometry, John Wiley & Sons, 1996.
[39] A.R. Denton, N.W. Ashcroft, Phys. Rev. A 43 (1991) 3161.
[40] M. Watanabe, in: A. Wieckowski, E.R. Savinova, C.G. Vayenas (Eds.), Catalysis and Electrocatalysis at Nanoparticle Surfaces, Marcel Dekker Inc., New York, 2003, p. 827.
[41] E. Peled, D. Golodnitsky, T. Ripenbein, N. Rudoy, A. Melman, Y. Rosenberg, Y. Lereah, 204th Meet. Electrochem. Soc., Orlando, FL, October 12–16, 2003 (Abstracts).